



A Neural Circuit for Memory Specificity and Generalization
Wei Xu and Thomas C. Südhof
Science **339**, 1290 (2013);
DOI: 10.1126/science.1229534

This copy is for your personal, non-commercial use only.

If you wish to distribute this article to others, you can order high-quality copies for your colleagues, clients, or customers by [clicking here](#).

Permission to republish or repurpose articles or portions of articles can be obtained by following the guidelines [here](#).

The following resources related to this article are available online at www.sciencemag.org (this information is current as of March 15, 2013):

Updated information and services, including high-resolution figures, can be found in the online version of this article at:

<http://www.sciencemag.org/content/339/6125/1290.full.html>

Supporting Online Material can be found at:

<http://www.sciencemag.org/content/suppl/2013/03/13/339.6125.1290.DC1.html>

This article **cites 40 articles**, 9 of which can be accessed free:

<http://www.sciencemag.org/content/339/6125/1290.full.html#ref-list-1>

This article appears in the following **subject collections**:

Neuroscience

<http://www.sciencemag.org/cgi/collection/neuroscience>

A Neural Circuit for Memory Specificity and Generalization

Wei Xu* and Thomas C. Südhof*

Increased fear memory generalization is associated with posttraumatic stress disorder, but the circuit mechanisms that regulate memory specificity remain unclear. Here, we define a neural circuit—composed of the medial prefrontal cortex, the nucleus reuniens (NR), and the hippocampus—that controls fear memory generalization. Inactivation of prefrontal inputs into the NR or direct silencing of NR projections enhanced fear memory generalization, whereas constitutive activation of NR neurons decreased memory generalization. Direct optogenetic activation of phasic and tonic action-potential firing of NR neurons during memory acquisition enhanced or reduced memory generalization, respectively. We propose that the NR determines the specificity and generalization of memory attributes for a particular context by processing information from the medial prefrontal cortex en route to the hippocampus.

Memories allow animals to adapt to a constantly changing environment. Memories are never completely precise but always partially generalized, which enables an animal to quickly and appropriately respond to novel stimuli that resemble a previous experience. The level of memory specificity and the degree of generalization are normally balanced. Generalization of fear memories protects animals

by alerting them to potential dangers when animals are exposed to situations that are similar to previously experienced harmful circumstances, but overgeneralization of fear memories can lead to inappropriate anxiety. This is evident with posttraumatic stress disorder (PTSD), in which the reexperiencing of a past trauma is triggered by cues existing in a normally safe environment (1). Similarly, overgeneralization of episodic memories is a consistent problem in patients with severe depression (2). Since its initial demonstration (3), memory generalization has been extensively characterized, and multiple theories to the hippocampus, which is critical for maintain-

ing the specificity of memories (4, 5), we recently found that the medial prefrontal cortex (mPFC) is essential for memory generalization (6). Specifically, we observed that global impairment of synaptic transmission in the mPFC unexpectedly caused overgeneralization of contextual fear memories. This observation is potentially interesting, because functional abnormalities of the mPFC have been consistently observed in patients with PTSD and other psychiatric disorders (1).

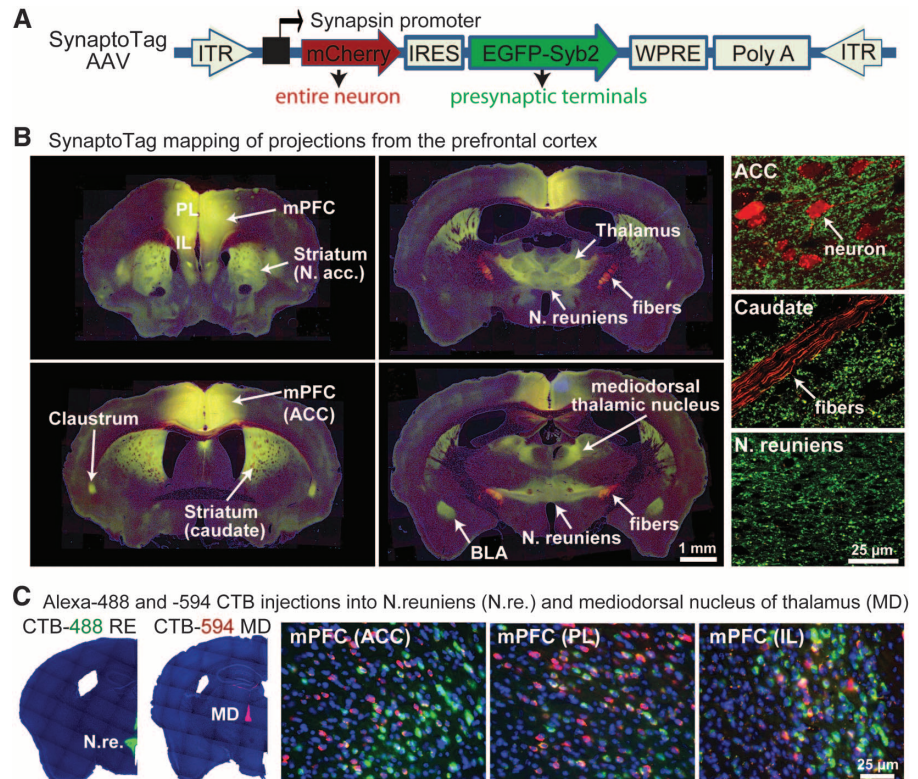
Mapping synaptic projections from the mPFC. The mPFC mediates the cognitive control of many high-level brain functions (7, 8). Consistent with such cognitive control, inactivation of synaptic transmission by expressing the light chain of tetanus toxin (TetTox) in the mPFC does not block fear memory, but leads to overgeneralization of such fear memory (6). However, it is unclear which synaptic projections from the mPFC to subcortical regions are critical for maintaining the proper balance between retention and generalization of fear memory details.

To quantitatively map the projections from the mPFC to subcortical regions, we developed a “SynaptoTag” adeno-associated virus (AAV), which coexpresses red fluorescent mCherry protein and enhanced green fluorescent protein (EGFP) fused to the synaptic vesicle protein synaptobrevin-2 (Fig. 1A) (9). Neurons infected with SynaptoTag AAV are filled with diffusible mCherry, which is present throughout their cytoplasm, including axon fibers. These neurons selectively localize green fluorescent synaptobrevin-2 to efferent synapses, allowing a quantitative assessment of

Department of Molecular and Cellular Physiology and Howard Hughes Medical Institute, Stanford University, 265 Campus Drive, Stanford, CA 94304-5453, USA.

*To whom correspondence should be addressed. E-mail: weixu@stanford.edu (W.X.); tcs1@stanford.edu (T.C.S.)

Fig. 1. Distinct mPFC neurons project to different synaptic targets. **(A)** Design of SynaptoTag AAV used for tracing synaptic connections. The synapsin promoter in the AAV drives bicistronic expression of soluble mCherry and a presynaptic EGFP–synaptobrevin-2 fusion protein (EGFP–Syb2). ITR, inverted terminal repeat; IRES, internal ribosome entry site; WPRE, woodchuck hepatitis posttranscriptional regulatory element. **(B)** SynaptoTag AAV mapping of mPFC projections. Representative low-resolution (left and middle panels) and high-resolution images (right panels) illustrate synaptic targets for mPFC neurons. Red mCherry labeling marks axonal fibers, whereas green EGFP labeling marks synapses projecting from the mPFC (yellow, coincident red and green labeling). BLA, basolateral nucleus of the amygdala; IL, infralimbic cortex; PL, prelimbic cortex; N. acc, nucleus accumbens (for complete sections, see fig. S1). **(C)** Retrograde labeling of mPFC neurons after injection of Alexa Fluor-488 and -594 labeled cholera toxin-B (CTB-488 and CTB-594) into the NR (N.re., green) and the mediadorsal thalamic nucleus (MD, red), respectively. Low-power micrographs (left panels) show injection areas, whereas high-power images (right panels) depict the three major mPFC regions. Most traced neurons were dominated by the presence of one fluorophore (for additional mPFC projections, see fig. S2).



the number of synapses formed in a target region by SynaptoTag AAV–infected neurons. This simple approach provides information about the distribution of both axonal fibers and synaptic terminals derived from a neuron.

We stereotactically injected SynaptoTag AAV into the mPFC of adult mice and imaged the localization of synapses formed by mPFC neurons 8 weeks later (Fig. 1B and fig. S1). Axons of mPFC neurons that were positive for mCherry formed a fiber bundle that extended caudoventrally through the corpus callosum, dorsal striatum, dorsal thalamus, hypothalamus, and midbrain structures. Axons continuously branched out of this bundle and formed synaptic connections with brain structures on the way. The intensity and density of the observed green synaptic puncta reflects the number of synaptic connections. Apart from a dense meshwork of synapses formed by mPFC neurons within the mPFC itself, mPFC neurons formed major synaptic pro-

jections in the mediodorsal striatum and nucleus accumbens, thalamus, claustrum, septohippocampal nucleus, and basolateral amygdala (Fig. 1B). In the thalamus, most projections were targeted to the mediodorsal nucleus (MD) and the nucleus reuniens (NR). The mPFC also sent substantial synaptic projections to the zona incerta, hypothalamic nuclei, midbrain, and periaqueductal gray.

The parallel connections of mPFC neurons to different subcortical nuclei raise the question of whether the same mPFC neurons project to multiple targets. Thus, we injected fluorescent cholera toxin B (CTB), tagged with Alexa Fluor-488 or Alexa Fluor-594 (Invitrogen, Carlsbad, California), into neighboring thalamic nuclei (the NR and the MD). We detected retrogradely labeled neurons in all three major subregions of the mPFC [the prelimbic cortex, the infralimbic cortex, and the anterior cingulate cortex (ACC)] (Fig. 1C and fig. S2). Most fluorescent mPFC neurons contained only one of

the two fluorophores, indicating that these neurons preferentially project to only one of the two neighboring thalamic regions examined. We also injected the fluorescent CTB tracers into the mediodorsal striatum and either the mediodorsal thalamic nucleus or the NR, and we observed a similar segregation of mPFC projection neurons (fig. S2).

Which mPFC projections control fear memory? We have previously observed overgeneralization of contextual fear memory induced by global expression of TetTox in the mPFC (6). Because distinct subpopulations of mPFC neurons project to different brain regions, it is unclear which of these projections participates in the circuit that controls fear memory generalization. To address this question, we used a trans-neuronally transported version of cre-recombinase that is fused to wheat-germ agglutinin (WGA-cre fusion protein) (10, 11).

We injected an AAV encoding a double-floxed, inverted EGFP and TetTox gene (2xFlx-TetTox) into the mPFC (Fig. 2A). This AAV expressed EGFP and TetTox only after inversion of the double-floxed expression cassette by cre-recombinase. At the same time, we injected a second AAV into one of the brain areas that are targeted by efferent synapses from the mPFC (Fig. 2B). The second AAV coexpressed red fluorescent mCherry and WGA-cre fusion protein (Fig. 2A). We then tested whether expression of WGA-cre in target areas for the mPFC activated EGFP and TetTox expression in the mPFC. We found that WGA-cre AAV injections specifically induced EGFP expression in the mPFC (Fig. 2B and fig. S3). Detection of WGA-cre-mediated trans-neuronal transport was made possible by modifications in the AAV vectors, especially by using a shorter synapsin promoter (~0.5 kb) and the AAV-DJ serotype (6). Substantially fewer mPFC neurons were labeled with EGFP by the WGA-cre/2xFlx-TetTox approach than were traced with CTB (Figs. 1C and 2B and figs. S3 and S4), suggesting that trans-synaptic WGA-cre transport is less efficient than retrograde labeling with an extracellular tracer. Quantifications showed that approximately one-third of the mPFC neurons projecting to the striatum were captured by trans-neuronal transport of WGA-cre from the target area (fig. S5). Despite its lower efficacy, we chose WGA-cre for our experiments instead of more efficacious rabies virus vectors (12), because rabies viruses in our hands induced rapid cytotoxicity, which may confound the interpretation of the behavioral results, whereas WGA-cre did not exhibit this problem.

We asked whether blocking specific projections from the mPFC to target areas alters fear memory generalization. We bilaterally injected the 2xFlx-TetTox AAV into the mPFC and the WGA-cre AAV into three target brain regions that receive synaptic inputs from the mPFC (the mediodorsal striatum, mediodorsal thalamic nucleus, and NR), as well as into the mPFC itself (as a positive control). We selected the mediodorsal striatum and the mediodorsal thalamic nucleus because they are major mPFC targets (Fig. 1B). We chose the NR because it forms an

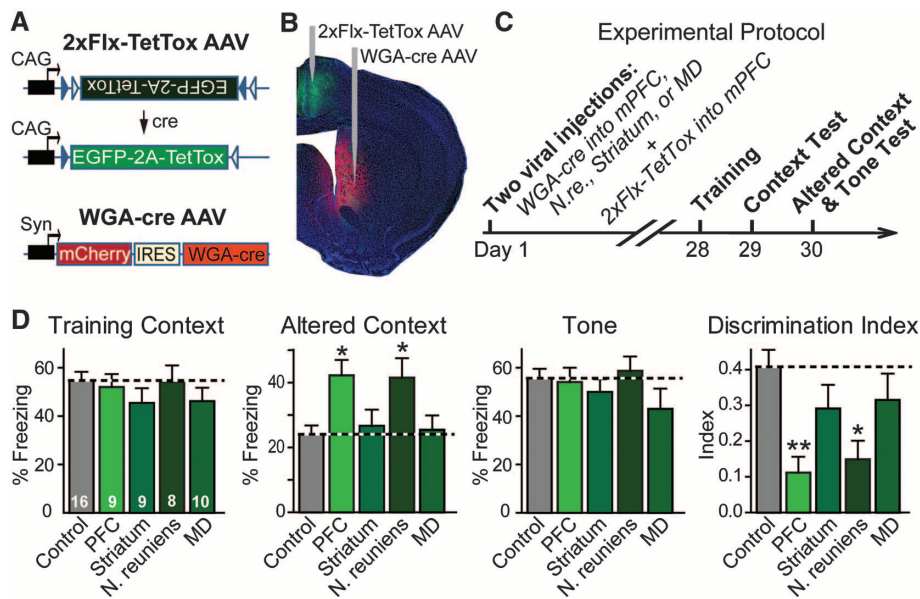


Fig. 2. mPFC projection to the NR controls memory specificity. **(A)** Design of AAVs used for inactivating synaptic transmission in subsets of projection neurons with specific synaptic targets. Double-floxed inverted TetTox-AAV (2xFlx-TetTox AAV) encodes bicistronic expression of EGFP for visualizing infected neurons and of TetTox for blocking synaptic transmission. The coding region of the double-floxed inverted TetTox-AAV is not translated until cre-recombinase flips the inverted coding region into the correct orientation. WGA-cre AAV mediates bicistronic expression of mCherry and WGA-cre. When this AAV infects a neuron, WGA-cre is trans-neuronally transferred to connected neurons, whereas mCherry is only expressed in the infected neuron. **(B)** Coronal brain section of a mouse injected with 2xFlx-TetTox AAV in the mPFC and with WGA-cre AAV in the dorsomedial striatum. The green EGFP fluorescence in the mPFC indicates that trans-synaptically transported WGA-cre activated expression of TetTox and EGFP in the mPFC. For high-magnification images, additional examples, and quantification of the trans-synaptic transport efficiency, see figs. S3 to S5. **(C)** Experimental protocol for analyzing the behavioral effects of selective TetTox expression in mPFC neurons that project to specific targets. 2xFlx-TetTox AAV was stereotactically injected into the mouse mPFC, and WGA-cre AAV was injected into the striatum, mediodorsal thalamic nucleus, NR, or mPFC (control, no WGA-cre AAV injection). Mice were tested 4 weeks later for contextual fear conditioning (context test), fear conditioning in an altered context to measure memory precision, and cued fear conditioning (tone test). For additional information, see fig. S6. **(D)** Fear conditioning measured with the experimental strategy described in (C) in multiple independent experiments (in the left panel, numbers in bars denote the number of mice analyzed). The discrimination index was calculated as the difference between the percentage of freezing in the training context and the altered context, divided by the sum of the two percentages. Data are means ± SEM (error bars); statistical significance (* $P < 0.05$; ** $P < 0.01$) was assessed by (i) two-way mixed-model analysis of variance (ANOVA) with Bonferroni's post-hoc test comparing the freezing levels or (ii) one-way ANOVA followed by Turkey's post-hoc test for the discrimination index. Horizontal dashed lines indicate the level of control groups.

anatomical link between the mPFC and the hippocampus (13, 14), both of which are essential for memory specificity (4–6), and because the NR has been shown to play a possible role in hippocampus-dependent learning and memory (15, 16).

Four weeks after viral injections, we performed fear conditioning tests (Fig. 2C and fig. S6). We trained the injected mice with three tone-foot-shock pairs in a conditioning chamber and then measured “freezing” sequentially, first in the training chamber to assess contextual fear memory, then in a similar but altered chamber to examine fear memory generalization, and finally, in response to the conditioning tone, in the altered chamber to measure cued fear memory (6). We quantified fear memory generalization as the discrimination index (the difference between freezing in the training and the altered context, divided by the sum of freezing in both conditions).

Global inactivation of the mPFC with TetTox did not impair cued or contextual fear conditioning but did induce overgeneralization of fear memories (Fig. 2D). Activation of TetTox, specifically in only mPFC neurons that projected to the striatum or the mediodorsal thalamic nucleus, had no effect on any parameter during fear conditioning, including memory generalization. However, activation of TetTox in only mPFC neurons that projected to the NR caused overgeneralization of fear memories, similar to what we observed with direct expression of TetTox in the mPFC (Fig. 2D). Given the incomplete efficiency of the retrograde transport of WGA-cre, our results do not exclude the possibility that the striatum and mediodorsal thalamic nucleus also play a more limited role in memory generalization, but our findings suggest that this role is not inhibited by partial inactivation of the mPFC projection to these nuclei. In contrast, partial inactivation of the mPFC projection to the NR is sufficient to produce overgeneralization of fear memories.

The NR bidirectionally controls fear memory generalization. To explore the control of fear memory generalization by the NR, we injected into the NR recombinant lentiviruses encoding either EGFP alone (control), TetTox, or a short hairpin RNA that suppresses neuroigin-2 expression (NL2 KD) (Fig. 3A and fig. S7A) (17–20). Whereas TetTox suppressed propagation of synaptic signals from the NR, the neuroigin-2 knockdown decreased synaptic inhibition of NR neurons (the NR lacks intrinsic inhibitory neurons releasing γ -aminobutyric acid and receives inhibitory inputs from other brain regions), thereby increasing propagation of synaptic signals from the NR (Fig. 3 and fig. S7).

Two weeks after viral injections, we measured fear conditioning (Fig. 3, D and E). Similar to the effects induced by TetTox in the mPFC, expression of TetTox in the NR caused an overgeneralization of contextual fear memory without significant effects on contextual or cued fear conditioning. This overgeneralization was specific for contextual memories, as the generalization of cued memories was not affected (fig. S8). In contrast to the effect of TetTox, suppression of neuroigin-2 expression reduced memory generalization (Fig. 3E).

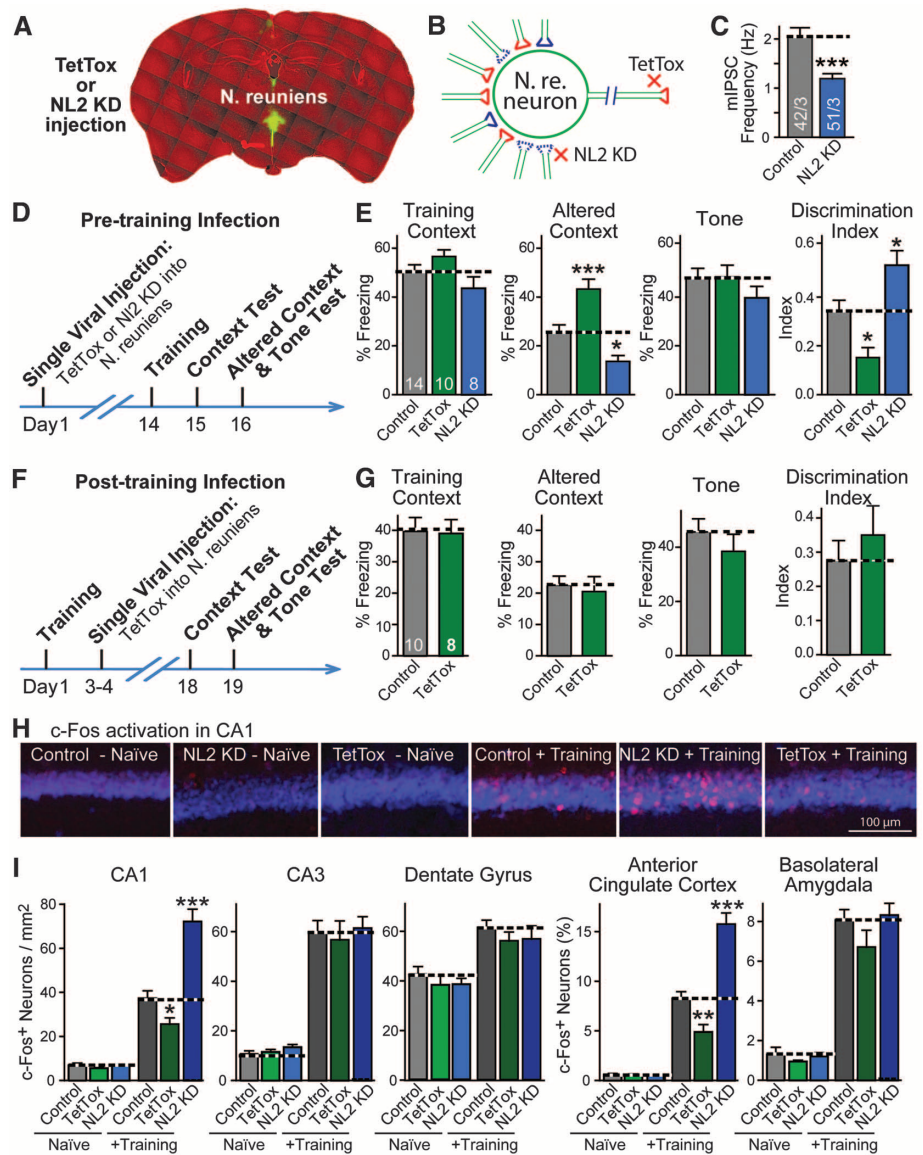


Fig. 3. The NR bidirectionally controls fear memory generalization. (A) Representative coronal brain section showing local expression of EGFP (green) after stereotaxic injection into the NR of lentiviruses encoding EGFP and TetTox or the neuroigin-2 knockdown (NL2 KD). (B) Schema of the effects of TetTox expression or of the neuroigin-2 knockdown on the activity of neurons in the NR. The neuroigin-2 knockdown decreases inhibition of NR neurons, thereby activating these neurons, whereas TetTox blocks synaptic outputs from NR neurons. (C) Effect of neuroigin-2 knockdown on the frequency of spontaneous inhibitory miniature synaptic events (mIPSCs), recorded in acute NR slices from mice that were injected with neuroigin-2 knockdown lentivirus (numbers in bars denote the number of neurons and mice analyzed, respectively). (D) Experimental protocol for testing fear memory after TetTox expression or neuroigin-2 knockdown in the NR. (E) Bidirectional changes in fear memory generalization by neuronal silencing with TetTox or neuronal activation with the neuroigin-2 knockdown. Mice injected with lentivirus expressing only EGFP were used as controls (numbers of mice are indicated in bars). (F and G) Same as (C) and (D), except that mice were injected with control or TetTox virus after fear conditioning training. (H and I) Effect of fear conditioning training and of TetTox expression or neuroigin-2 knockdown in the NR on the activity levels of neurons in different adult brain regions. Control, TetTox, or the neuroigin-2 knockdown lentiviruses were injected into the NR of target mice. Mice were subjected to fear conditioning training (+Training) or received no training (naïve) and were sacrificed 90 min after training. Brain sections were stained for c-Fos (red) to measure neuronal activation and NeuN to label all neuronal nuclei (blue). (H) Representative images of the hippocampal CA1 region. (I) Quantification of c-Fos expression in the indicated brain regions ($n = 12$ to 18 brain sections from four mice in each group; for additional data, see figs. S11 and S12). Data shown are means \pm SEM (error bars). Statistical significance ($*P < 0.05$; $**P < 0.01$; $***P < 0.001$) was assessed by two-tailed Student's t test [(C) and (G)], two-way ANOVA followed by Bonferroni's post-hoc test [(E), comparing freezing levels, and (I)], or one-way ANOVA followed by Turkey's post-hoc test [discrimination index in (E)]. Horizontal dashed lines indicate the level of control groups.

Does the NR determine the precision of memory during memory acquisition and/or during memory retrieval? To address this question, we injected lentiviruses expressing TetTox into the NR after fear conditioning and measured fear memories 2 weeks later (Fig. 3, F and G). Expression of TetTox after training had no effect on memory generalization, establishing the specificity of the effects observed by TetTox on the generalization of fear memory during the acquisition stage.

The mPFC, NR, and hippocampus constitute a memory generalization circuit. The NR directly projects to the hippocampus and back to the mPFC (13, 14), and the hippocampus, in turn, also projects to the mPFC (21), thus creating a closed loop with the projection from the mPFC to the NR (Fig. 1). In mapping experiments using SynaptoTag AAV injections into the NR and the hippocampus, we confirmed these conclusions (figs. S9 and S10). A major question, however, is how much the activity of NR neurons actually influences neuronal excitation in the hippocampus; that is, whether this is a major signaling pathway during memory acquisition.

Previous studies indicate that memories with high specificity involve a high level of engagement of the hippocampus (22). Thus, we examined whether enhanced fear generalization upon TetTox expression or reduced fear generalization following neuroigin-2 suppression in the NR are associated with corresponding changes in the activation of hippocampal neurons and whether such changes are specific to these neurons. We subjected control mice and mice with TetTox expression or neuroigin-2 knockdown in the NR to fear conditioning training, and we analyzed c-Fos expression in multiple brain regions 90 min afterward.

Consistent with previous reports (23, 24), c-Fos-positive neurons were increased after training in multiple brain regions, including the hippocampus, mPFC, amygdala, ventral tegmental area, and periaqueductal gray in control mice (Fig. 3, H and I, and figs. S11 and S12). Expression of TetTox or knockdown of neuroigin-2 in the NR had little effect on the basal c-Fos expression in any brain region. However, TetTox expression significantly and selectively decreased c-Fos

activation in the CA1 region of the hippocampus and in the ACC of the mPFC, whereas the neuroigin-2 knockdown significantly enhanced the effects of training on c-Fos expression in these two brain regions (Fig. 3I and fig. S12).

Activity patterns of NR neurons control memory specificity. To directly test the role of the NR in balancing the precision of contextual fear memories, we stimulated firing of NR neurons in behaving mice during memory acquisition using optogenetics. We expressed the channelrhodopsin-derivative ChIEF (25) in the NR and stimulated NR neurons via an implanted optical fiber (Fig. 4A). Electrophysiological experiments have shown that ChIEF exhibits fast kinetics and allows action-potential stimulation at frequencies of up to 50 Hz (25).

We used either tonic 4-Hz stimulus trains or phasic 15-pulse stimulus bursts to stimulate NR neurons during fear conditioning training (Fig. 4B) (26, 27). Similar to the TetTox and neuroigin-2 knockdown manipulations in the NR, neither the phasic nor the tonic NR stimulation had detectable effects on contextual or cued fear conditioning (Fig. 4C). However, these stimulations induced opposite changes in fear memory generalization. Phasic NR stimulation during training caused increased freezing in the altered context (i.e., produced overgeneralization of fear memory). In contrast, tonic NR stimulation induced decreased freezing in the altered context (i.e., a reduction in fear generalization) (Fig. 4C).

Because the two stimulation patterns we used represent, in principle, the same manipulation—optogenetic stimulation of NR firing—but result in opposite effects, these patterns control for each other, ruling out the possibility that the optogenetic manipulation simply impairs the functions of the NR instead of specifically stimulating it. Previous studies have shown that stimulation of the inputs from the NR to the hippocampus produces sub-threshold depolarization of CA1 pyramidal cells but above-threshold stimulation of inhibitory interneurons (28). The different behavioral phenotypes produced by the distinct stimulation patterns of NR neurons might arise from the relative impact of their stimulation on their downstream excitatory versus inhibitory neurons. Recent evidence indicates that the activity of the NR correlates with hippocampal oscillations, suggesting that the different behavioral effects may be related to changes in hippocampal oscillations (29).

Summary. Here, we establish that the mPFC controls memory specificity via signaling to the NR that, in turn, signals to the hippocampus and also back to the mPFC. The generalization of hippocampus-dependent memories is often discussed in the framework of complementary learning systems theory (30, 31). In this theory, the hippocampus keeps separate representations of individual memory episodes (specific memories), whereas the cortex abstracts common features from multiple memories. Through systems consolidation, in which memories are transferred from the hippocampus to the cortex, memories become generalized. Highly specific memories are proposed

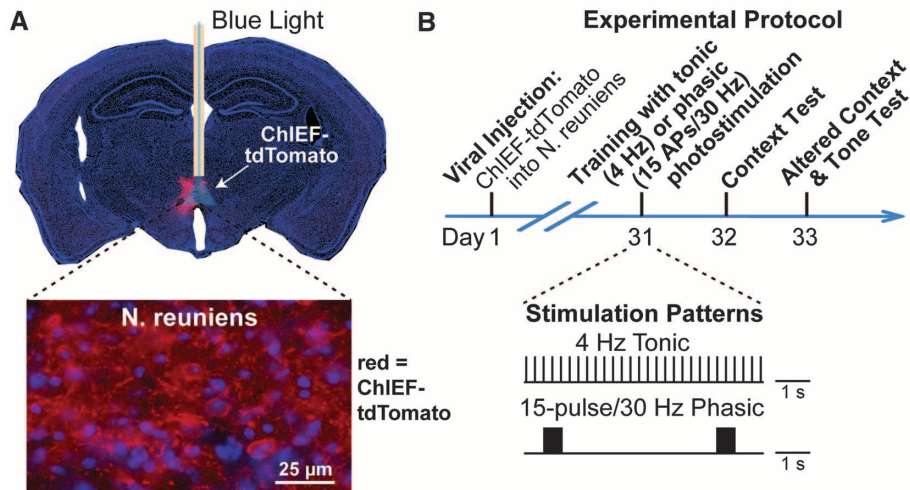
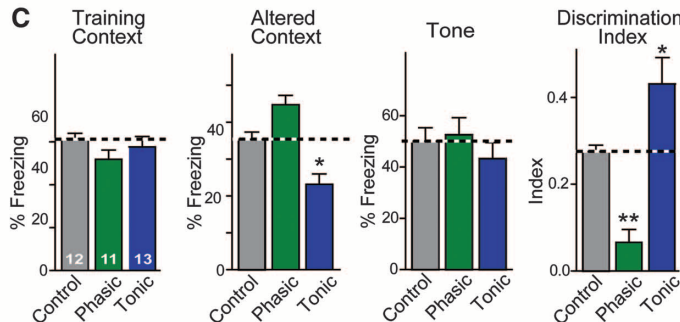


Fig. 4. Firing pattern of NR neurons dictates memory generalization. (A) (Top) Coronal brain section illustrating expression of ChIEF-tdTomato (red fluorescent channelrhodopsin) in the NR. (Bottom) High-magnification micrograph showing ChIEF-tdTomato expressing NR neurons and their axonal fibers. (B) Experimental protocol for testing the effect of different optogenetic stimulation patterns of NR neurons on fear conditioning behavior, with the stimulation patterns illustrated below the time diagram. NR neurons were stimulated throughout the 6-min training period by either a 4-Hz tonic stimulation or a 30-Hz phasic stimulation administered for 0.5 s every 5 s. Stimulus light pulses lasted 15 ms. (C) Tonic and phasic optogenetic stimulation produced opposite effects on fear memory generalization. Control mice also expressed channelrhodopsin and contained an implanted optical fiber, but were not stimulated. Data shown are means \pm SEM (error bars); numbers in bars indicate the number of mice analyzed. Statistical significance ($*P < 0.05$; $**P < 0.01$) was assessed by two-way mixed-model ANOVA followed by Bonferroni's post-hoc test comparing the freezing levels or by one-way ANOVA followed by Turkey's post-hoc test for the discrimination index. Horizontal dashed lines indicate the level of control groups.



to be maintained through “pattern separation,” but can be generalized during retrieval through “pattern completion” (32, 33). Complementary learning systems theory provides a plausible account of the time-dependent generalization of memories after memory acquisition and their generalization upon memory retrieval (34–36), but this theory does not explain how memory generalization is controlled during acquisition. Taking advantage of the temporal precision of optogenetic stimulations, we found that the mPFC-NR-hippocampus circuit controls memory specificity and generalization during acquisition (Fig. 4).

Because memories are not composed of simple unitary traces but rather of flexible combinations of attributes or features of the remembered objects or situations (37, 38), generalization of memories may stem from overlap between the representations of the attributes and/or features of memories (39, 40). Different attributes of an object may not be remembered equally. For example, after seeing a baseball with a player’s autograph (Fig. 5B), readers may memorize distinct combinations of the baseball’s features to form memories with different levels of specificity. When only the most prominent attributes are remembered, its memory representation is more likely to overlap with that of another memory and become generalized. But when more features are remembered, the overall representation is less likely to overlap with other memory representations and, hence, becomes more specific. A plausible model that accounts for our

findings is that the NR may exert a persistent regulation of the excitability of hippocampal neurons, thereby controlling memory generalization (28). Increased excitability may allow less prominent memory features to be incorporated into overall memories by facilitating the firing or synaptic plasticity of CA1 neurons (fig. S13). Memories with more detailed attributes will then become more specific. This overall idea agrees with the general functions proposed for midline thalamic structures: Instead of relaying specific sensory information, they are thought to adjust the activity level of cortical structures (including the hippocampus and mPFC) (41). Studies of hippocampal place cells indicate that these cells undergo substantial “remapping” when encoding similar memories, especially in the CA3 region. Through remapping, subtle changes in the environment could produce profound alterations of a memory representation in the hippocampus, thereby increasing the distinction between similar memories (42). Thus, the mPFC-NR-hippocampus circuit may regulate memory generalization by actively controlling remapping. Notably, hippocampal remapping is modulated by motivational and emotional states (42, 43). Because the mPFC is centrally involved in the motivational and emotional states of an animal (7, 8), the mPFC-NR pathway may convey the motivational and emotional value of the attributes of a memory to the hippocampus for memory encoding, which, in turn, may underlie the regulation of memory generalization during acquisition.

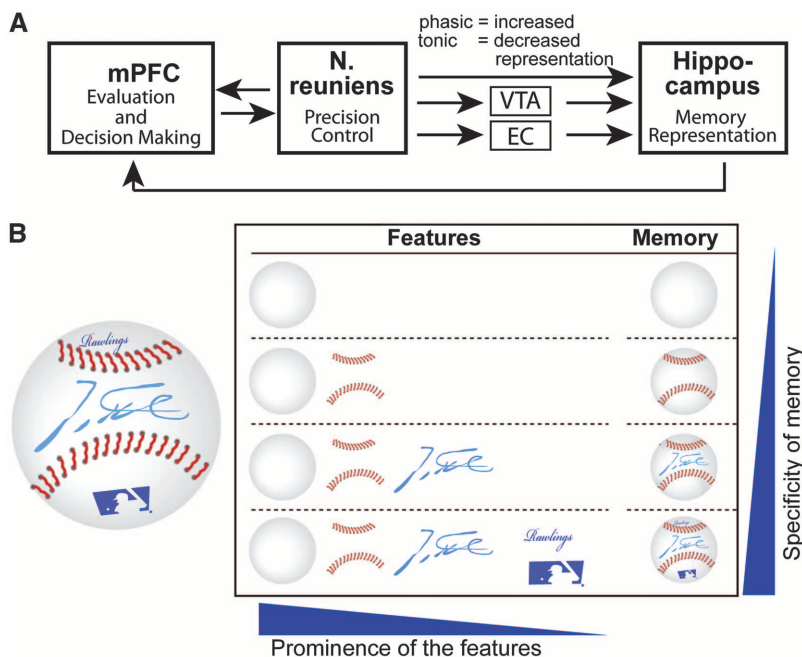


Fig. 5. Model for the mechanism of the NR’s control of memory generalization. **(A)** Schematic diagram of the synaptic interactions between the mPFC, NR, and hippocampus in controlling memory generalization. VTA, ventral tegmental area; EC, entorhinal cortex. **(B)** Illustration of the modular composition of memory features. We posit that memories differentially incorporate a composite of specific attributes. The more prominent a feature is, the more likely it is to be included in memory, as illustrated here with a baseball containing additional features besides “ballness.” We propose that NR neurons control memory generalization by regulating the number of features that are incorporated into a memory. For a more detailed discussion, see fig. S13.

References and Notes

- A. L. Mahan, K. J. Ressler, *Trends Neurosci.* **35**, 24 (2012).
- I. H. Gotlib, J. Joormann, *Annu. Rev. Clin. Psychol.* **6**, 285 (2010).
- J. B. Watson, R. Rayner, *Am. Psychol.* **55**, 313 (2000).
- P. W. Frankland, V. Cestari, R. K. Filipkowski, R. J. McDonald, A. J. Silva, *Behav. Neurosci.* **112**, 863 (1998).
- F. G. Freeman, N. R. Kramarcy, J. Lee, *Physiol. Behav.* **11**, 273 (1973).
- W. Xu *et al.*, *Neuron* **73**, 990 (2012).
- J. W. Dalley, R. N. Cardinal, T. W. Robbins, *Neurosci. Biobehav. Rev.* **28**, 771 (2004).
- S. P. Wise, *Trends Neurosci.* **31**, 599 (2008).
- Experimental procedures are explained in the materials and methods section of the supplementary materials on Science Online.
- J. M. Braz, B. Rico, A. I. Basbaum, *Proc. Natl. Acad. Sci. U.S.A.* **99**, 15148 (2002).
- V. Gradinaru *et al.*, *Cell* **141**, 154 (2010).
- F. Osakada *et al.*, *Neuron* **71**, 617 (2011).
- R. P. Vertes, *Neuroscience* **142**, 1 (2006).
- R. P. Vertes, W. B. Hoover, K. Szigeti-Buck, C. Leranah, *Brain Res. Bull.* **71**, 601 (2007).
- M. J. Dolleman-van der Weel, R. G. Morris, M. P. Witter, *Brain Struct. Funct.* **213**, 329 (2009).
- M. Loureiro *et al.*, *J. Neurosci.* **32**, 9947 (2012).
- We chose lentiviruses for these experiments because they infect a small area of less than 0.8 mm in diameter (Fig. 3A). TetTox inactivates all synaptic outputs from the NR. Neuroligin-2 is a synaptic adhesion molecule that is exclusively expressed in inhibitory synapses (18), and inactivation of neuroligin-2 depresses the function of a subset of inhibitory synapses (19, 20).
- F. Varoqueaux, S. Jamain, N. Brose, *Eur. J. Cell Biol.* **83**, 449 (2004).
- J. R. Gibson, K. M. Huber, T. C. Südhof, *J. Neurosci.* **29**, 13883 (2009).
- A. Pouloupos *et al.*, *Neuron* **63**, 628 (2009).
- L. W. Swanson, *Brain Res.* **217**, 150 (1981).
- B. J. Wiltgen *et al.*, *Curr. Biol.* **20**, 1336 (2010).
- I. Goshen *et al.*, *Cell* **147**, 678 (2011).
- S. Milanovic *et al.*, *Brain Res.* **784**, 37 (1998).
- J. Y. Lin, M. Z. Lin, P. Steinbach, R. Y. Tsien, *Biophys. J.* **96**, 1803 (2009).
- Because only limited information about the natural firing patterns of NR neurons is available (27–29), we first explored stimulation patterns to identify an optimal regimen. We found that tonic 4-Hz stimulus trains and phasic 15-pulse stimulus bursts (delivered at 30 Hz with 5-s intervals) produced significant but distinct behavioral effects, leading us to use these two stimulation paradigms for our experiments.
- G. J. Morales, E. J. Ramcharan, N. Sundararaman, S. D. Morgera, R. P. Vertes, *Conf. Proc. IEEE Eng. Med. Biol. Soc.* **2007**, 2480 (2007).
- M. J. Dolleman-Van der Weel, F. H. Lopes da Silva, M. P. Witter, *J. Neurosci.* **17**, 5640 (1997).
- Y. Zhang, T. Yoshida, D. B. Katz, J. E. Lisman, *J. Neurophysiol.* **107**, 3181 (2012).
- D. Kumaran, J. L. McClelland, *Psychol. Rev.* **119**, 573 (2012).
- J. L. McClelland, B. L. McNaughton, R. C. O’Reilly, *Psychol. Rev.* **102**, 419 (1995).
- T. J. McHugh *et al.*, *Science* **317**, 94 (2007).
- T. Nakashiba *et al.*, *Cell* **149**, 188 (2012).
- C. C. Perkins Jr., R. G. Weyant, *J. Comp. Physiol. Psychol.* **51**, 596 (1958).
- B. J. Wiltgen, A. J. Silva, *Learn. Mem.* **14**, 313 (2007).
- Y. Zhou, D. C. Riccio, *Learn. Motiv.* **27**, 400 (1996).
- H. Eichenbaum, *Neuron* **44**, 109 (2004).
- H. Eichenbaum, P. Dudchenko, E. Wood, M. Shapiro, H. Tanila, *Neuron* **23**, 209 (1999).
- M. W. Howard, M. S. Fotedar, A. V. Datey, M. E. Hasselmo, *Psychol. Rev.* **112**, 75 (2005).
- S. M. McTighe, R. A. Cowell, B. D. Winters, T. J. Bussey, L. M. Saksida, *Science* **330**, 1408 (2010).
- H. J. Groenewegen, H. W. Berendse, *Trends Neurosci.* **17**, 52 (1994).
- L. L. Colgin, E. I. Moser, M. B. Moser, *Trends Neurosci.* **31**, 469 (2008).
- M. A. Moita, S. Rosis, Y. Zhou, J. E. LeDoux, H. T. Blair, *J. Neurosci.* **24**, 7015 (2004).

Acknowledgments: We thank the following colleagues for providing plasmids and advice: M. Fucillo and J. Ko (neuroigin-2 knockdown constructs), J. Burre (EGFP-synaptobrevin-2 construct), C. Acuna and R. Tsien (ChIEF-tdTomato), S. Lammel (advice on optogenetics), and K. Diesseroth (WGA-cre plasmid). This study was supported by grants from the Simons Foundation (177850), the

National Institute of Mental Health (P50 MH086403), and the National Institute of Neurological Disorders and Stroke (NS077906).

Supplementary Materials

www.sciencemag.org/cgi/content/full/339/6125/1290/DC1
Materials and Methods

Figs. S1 to S13
References

30 August 2012; accepted 1 February 2013
10.1126/science.1229534

REPORTS

Spin Torque–Generated Magnetic Droplet Solitons

S. M. Mohseni,^{1,2} S. R. Sani,^{1,2} J. Persson,² T. N. Anh Nguyen,¹ S. Chung,^{1,3}
Ye. Pogoryelov,³ P. K. Muduli,^{3,4} E. Iacocca,³ A. Eklund,⁵ R. K. Dumas,³ S. Bonetti,^{1,6}
A. Deac,⁷ M. A. Hoefer,⁸ J. Åkerman^{1,2,3*}

Dissipative solitons have been reported in a wide range of nonlinear systems, but the observation of their magnetic analog has been experimentally challenging. Using spin transfer torque underneath a nanocontact on a magnetic thin film with perpendicular magnetic anisotropy (PMA), we have observed the generation of dissipative magnetic droplet solitons and report on their rich dynamical properties. Micromagnetic simulations identify a wide range of automodulation frequencies, including droplet oscillatory motion, droplet “spinning,” and droplet “breather” states. The droplet can be controlled by using both current and magnetic fields and is expected to have applications in spintronics, magnonics, and PMA-based domain-wall devices.

Dissipative solitons are localized excitations realized by a balance between nonlinearity, dispersion, gain, and loss (*1, 2*). They can be experimentally observed in optical (*3, 4*), chemical (*5, 6*), granular (*7*), and liquid (*8*) dissipative systems. Large amplitude nanoscale dynamics in magnetic thin films with perpendicular magnetic anisotropy (PMA) inherently possess all mechanisms supporting dissipative solitons except for gain. Spin-transfer torque (STT) (*9–12*) provides for the injection of angular momentum from spin-polarized electrons into a magnet. Using STT as the gain mechanism in nanocontact (NC)-based spin-torque oscillators (STOs), a magnetic dissipative soliton—the so-called “magnetic droplet”—was recently proposed (*13–15*). Using NC-STOs, we created and investigated magnetic droplet dynamics experimentally.

Classical conservative solitons, such as light pulses in a virtually lossless optical fiber, preserve their shape by balancing the opposing ef-

fects of dispersion (spreading) and nonlinearity (focusing). Similarly, if damping is ignored the Landau-Lifshitz equation for an extended two-dimensional magnetic thin film with PMA can sustain a family of conservative magnetic solitons, known as “magnon drops” (*16, 17*). All spins in a magnon drop precess in phase around the film normal, with a precession angle $0 < \Theta(0) < \pi$ at the center of the drop and $0 < \Theta(r) < \Theta(0)$ decreasing exponentially fast, with radius to 0 in the far field. The family of stationary magnon drops can be parameterized by the precessional frequency f_0 , satisfying $f_{\text{Zeeman}} < f_0 < f_{\text{FMR}}$, where f_{FMR} is the ferromagnetic resonance (FMR) frequency, and f_{Zeeman} is the Zeeman frequency. Magnon drops can be strongly nonlinear, exhibiting almost fully reversed cores [$\Theta(0) \rightarrow \pi$] for f_0 close to f_{Zeeman} . Whereas conservative magnon drops balance exchange (dispersion) with anisotropy (nonlinearity) for each f_0 , the dissipative magnetic droplet must also balance energy gain (STT) with dissipation (damping), singling out a particular droplet precession frequency for a given drive current and applied field (Fig. 1C) (*13*). More generally, dissipative soliton systems, such as the NC-STOs studied here, are natural environments for studying pattern formation. Dissipative solitons are often robust attractors and can exhibit exotic dynamics, such as time-periodic breathing (*1*). It has been claimed that NC-STOs with in-plane anisotropy and applied field exhibit nonlinear localization in the form of a weakly nonlinear spin wave bullet with precession angles much less than 90° (*18, 19*). In contrast, the fully nonlinear dissipative droplet studied here neces-

sarily involves precession angles greater than 90° (*13*), exhibiting a clear experimental signature and rich nonlinear behavior.

To test the theoretical predictions for a magnetic droplet (*13*), we fabricated NC-STOs based on orthogonal pseudospin valve stacks (Fig. 1C), in which the magnetization of the Co fixed layer lies in the plane for zero applied field, whereas that of the Co/Ni multilayer free layer lies along the film normal because PMA is sufficiently strong to overcome the demagnetization field (*20–22*).

The field dependence of the microwave signal from a NC-STO with 63-nm NC diameter in low to moderate perpendicular fields (Fig. 1A) shows the expected linear FMR-like field dependence (*20, 21*). However, at a critical field of $\mu_0 H_{\text{droplet}} = 0.65$ T, the precession frequency exhibits a dramatic drop to a frequency that lies between the Zeeman and FMR frequencies, with a simultaneous jump in the integrated power (*P*). A similarly dramatic transition can be observed (Fig. 1B) as a function of current in a constant field of 0.8 T with similar changes in frequency and power. To gain further insight into the magnetic state as a function of field and current, the magnetoresistance $\{\text{MR} = [R(H) - R(H = 0)] / R(H = 0)\}$, where R is the device resistance was measured both at -6 mA and at a lower current of -1 mA (Fig. 1A, inset). Below 0.65 T, the MR exhibits an identical linear decrease for both currents, which is consistent with a linearly increasing out-of-plane component of the fixed layer magnetization and an increasingly parallel state of the NC-STO. At exactly $\mu_0 H_{\text{droplet}} = 0.65$ T, MR [current (I) = -6 mA] exhibits a jump of 0.1%, and its field dependence changes sign; the NC-STO state thus becomes increasingly antiparallel with increasing field. Contrarily, MR (I = -1 mA) does not show any sign of transition and continues to decrease linearly, eventually saturating in a field of 1.6 to 1.8 T (fig. S1) (*22*), which is consistent with the expected saturation field for the Co layer.

Both the dynamic and static observations are consistent with the formation of a magnetic droplet in the free layer. The large drop in frequency and the sign change of the field-dependent resistance further indicate a substantially reversed central region. This is corroborated by the large increase in microwave power because a reversed droplet will have a large area of spins precessing around the equator, whereas the precession angle of the FMR-like mode is very limited close to the threshold for STO dynamics (*10, 13*). Last, according to the theory of the magnetic droplet, its

¹Materials Physics, School of Information and Communication Technology, KTH Royal Institute of Technology, Electrum 229, 164 40 Kista, Sweden. ²NanOsc AB, Electrum 205, 164 40 Kista, Sweden. ³Department of Physics, University of Gothenburg, 412 96 Gothenburg, Sweden. ⁴Department of Physics, Indian Institute of Technology Delhi, New Delhi 110016, India. ⁵Devices and Circuits, School of Information and Communication Technology, KTH Royal Institute of Technology, Electrum 229, 164 40 Kista, Sweden. ⁶Department of Physics, Stanford University, Stanford, CA 94305, USA. ⁷Institute of Ion Beam Physics and Materials Research, Helmholtz-Zentrum Dresden-Rossendorf e. V., 01314 Dresden, Germany. ⁸Department of Mathematics, North Carolina State University, Raleigh, NC 27695, USA.

*To whom correspondence should be addressed. E-mail: johan.akerman@physics.gu.se